P 109

Offshore sub-basalt exploration using CSEM and MT

Krishna Kumar, Deepankar Borgohain, Jan Petter Morten, Frida Mrope, Martin Panzner and Deepak Kumar, (EMGS)*

Summary

Seismic sub-basalt imaging is challenging and leads to a large degree of uncertainty. This paper considers how marine EM methods (CSEM and MT) can reduce uncertainty by providing structural and resistivity information about basalt and the sediments below. In order to demonstrate the capability of this technology, we will present two recent studies: 1) Imaging of synthetic data from a realistic model based on well-log and seismic data, and, 2) a field data example. These studies show how EM data can improve interpretation certainty with structural and quantitative information in the inverted resistivity models and potentially improve velocity models for seismic imaging.

Keywords: *Sub-basalt imaging, CSEM, MT, anisotropy*

Introduction

Basalts are extrusive igneous rocks that can be found worldwide. There may be sediments below or within basalts that may contain hydrocarbons, and basalt can also act as a seal for hydrocarbon reservoirs.

With seismic, one can usually establish the top basalt accurately, but due to heterogeneities in the basalt layer and the high seismic velocities it can be challenging to image the base of basalt accurately or the sediments below (Fliender and White, 2001; Thacher et al., 2013) and EM methods can play a significant role in mapping the base of basalt. Earlier, Jegen et al. (2002) showed that MT can be used to map sedimentary basins below basalt. Houtot et al. (2002) indicated that seismic + MT is good enough to image a sedimentary package within basalt with a very good resolution for thick basalt. Later MacGregor (2003) presented that MT can image very thick basalt layers. Colombo et al., (2011) demonstrated that MT added value to the exploration of complex geological basalt plays covering an area in NW Saudi Arabia. Also Pandey et al. (2008) indicated that onshore MT provides help to image highly anisotropic basalt in Deccan Traps, India.

In this paper, we focus on the role of varying thickness and electrical anisotropy of the basalt. We consider two cases, (1) a synthetic data study based on a realistic model (Herredsvela et al., 2012) and (2) a field data example from West of Shetland.

Synthetic Basalt Model

The model in Figure 1 has a highly anisotropic basalt layer on the EM data scale with varying thickness from meters to kilometers, and also with detailed structure underneath the basalt. The internal structure in the basalt is based on the observations from well logs and seismic. The information used to construct this model makes it analogue to a realistic scenario. Figure 1 shows the vertical resistivity component. The water depth varies from 300 to 350 m and the model consists of a basaltic delta of variable thickness from 200 m to 2 km.

Due to the low-frequency of the EM signal, homogeneous effective basalt models were considered to represent the internal structures. A TIV anisotropic resistivity model is considered. A large value for the anisotropy ratio was used, ρ_V/ρ_H ~7 with vertical resistivity 55 Ωm and horizontal resistivity 8 Ωm. The effective value for the horizontal resistivity represents a lower estimate, in order to study the performance of EM imaging for a difficult case with little horizontal resistivity contrast to the background. The resistivity of the sub basalt sediments is 6 Ωm. The large basalt anisotropy on the EM data scale

Unit E-15.2-4, 15th Floor, East Wing, Wisma Rohas Perkasa, No.9 Jalan P. Ramlee, 50250, Kuala Lumpur, Malaysia, email: dborgohain@emgs.com

arises due to alternating conductive and resistive layers in the vertical direction. The data for this model is generated with the algorithm described by Maaø (2007).

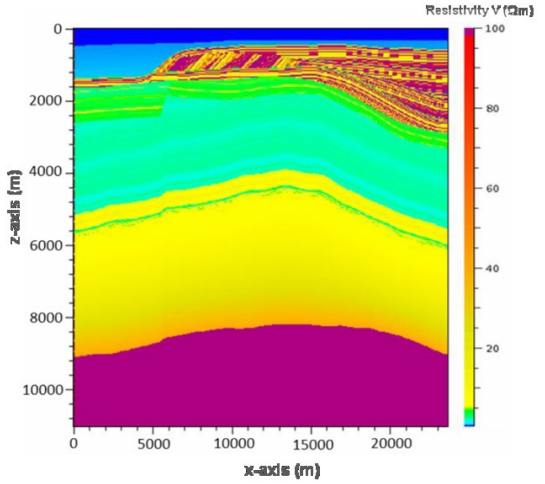

Figure 1: Vertical resistivity section of synthetic basalt model with detailed internal structure (after Herredsvela et al., 2012)

Herredsvela et al. (2012) show that for the basalt case in shallow water, inline CSEM data is equally sensitive to both thick and thin basalt. For ultra-deep water (Morten et al., 2011), the CSEM broadside configuration helps to image thick basalt. These dependencies are important to take into account during survey planning.

Inversion results

We use the 2.5D CSEM inversion described by Hansen and Mittet (2009) and Occam 2D MT inversion described by Constable et al. (1987) to invert the dataset. The CSEM inversion is anisotropic whereas the MT inversion is isotropic. MT is a plane wave phenomenon and has much less sensitivity to vertical resistivity in comparison to horizontal resistivity. Flooded basalt models (where basalts are extending down to the bottom of the model) with an exact basalt top are used as the initial model for inversion because the top can typically be accurately imaged with seismic. Both inline and broadside data are used in the CSEM inversion.

Only CSEM offsets that can be measured with good signal-to-noise ratio are used for inversion. Three frequencies 0.11, 0.39 and 0.88 Hz are used. Figure 2 and 3 show CSEM inverted models for vertical and horizontal resistivity. Both images clearly show the basalt, but the vertical resistivity is more sensitive to the thin basalt in comparison to the horizontal resistivity. The layers beneath the basalt are not distinguishable due to the limited frequency band.

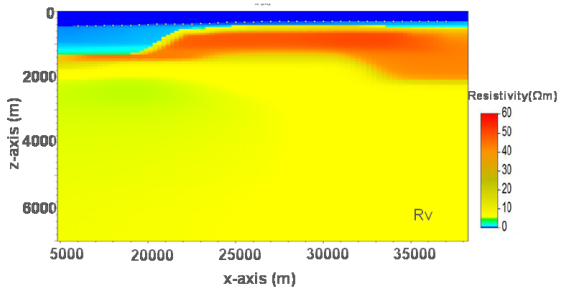

Figure 2: Vertical resistivity model after 2.5D CSEM inversion.

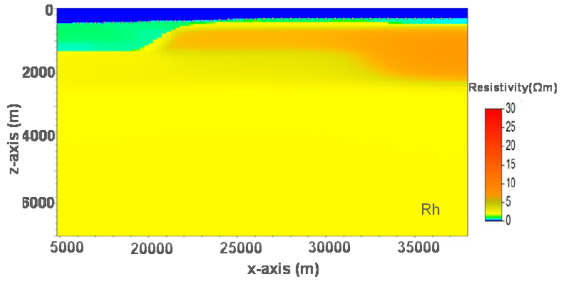

Figure 3: Horizontal resistivity model after 2.5D CSEM inversion.

For MT inversion 23 frequencies were used between 1.43 to 10^{-4} Hz. The inverted model is shown in Figure 4.

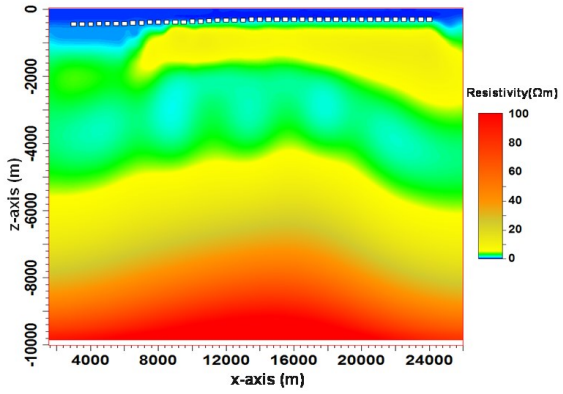

Figure 4: 2D MT inversion model.

MT inversion is not sensitive to the thinnest part of the basalt but to the base of the basalt and recovers the sub-basalt sediments. The low frequencies play a significant role in deep imaging.

Real Field Example (West of Shetland)

We now go on to consider a field data example for basalt imaging. Figure 5 shows the seismic image of this area where only the top basalt can be interpreted with confidence. No structural information is clearly visible underneath.

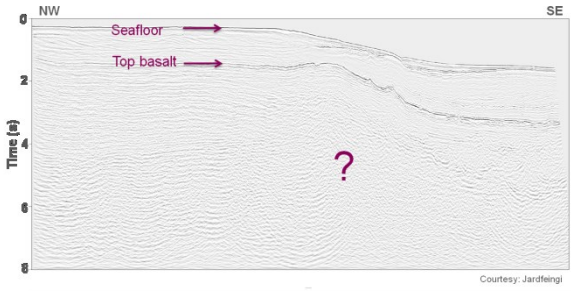

Figure 5: Seismic image in the area

CSEM and MT data were acquired in this region by EMGS. A total of 84 seabed receivers recorded signals along the 2D line shown in Figure 6. Frequencies used for MT inversion were between 0.354 to 0.007 Hz with an initial model of a 1 Ωm half space. CSEM frequencies were 0.2, 0.6, 1.0, 1.4 Hz.

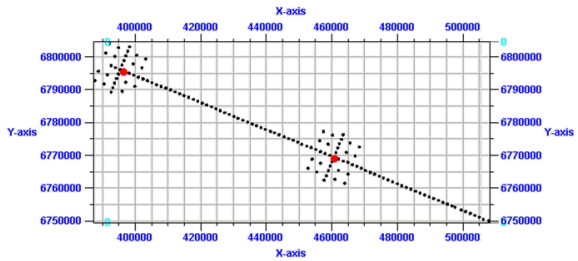

Figure 6: Map view of the survey layout.

Seismic and well-log data is only shown to demonstrate the effectiveness of EM methods and was not used as a constraint or for the start model. For the thin basalt section, the vertical resistivity model provides the best results, while for thick basalt the horizontal resistivity is more effective. This is because CSEM data is more sensitive to thin resistors in the vertical resistivity component.

In MT inversion, the base of basalt is not imaged clearly in this case. Nonetheless, MT provides good general background information especially for the basement and this information is useful for start model building for CSEM inversion. Figure 7 shows the inversion result from the MT inversion.

Start models for 3D CSEM inversion are based on 2.5D CSEM and 2D MT inversions, integrating basic resistivity trends. Anisotropic 3D CSEM inversion resistivity images, vertical and horizontal, are presented in Figure 8(a) and 8(b) respectively.

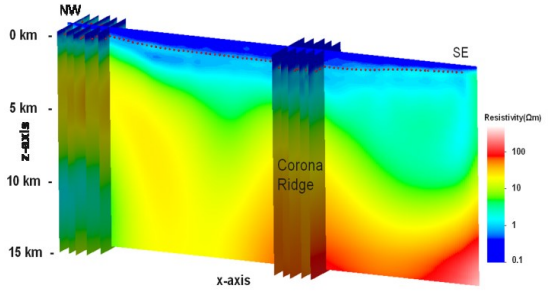

Figure 7: MT inversion (TE+TM)

a

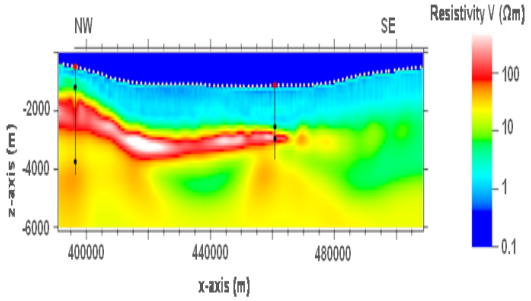

b

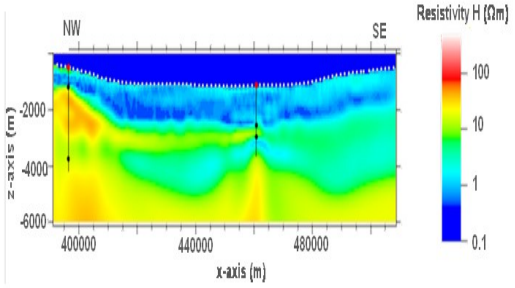

Figure 8: Unconstrained 3D CSEM inversion images; a) vertical resistivity, b) horizontal resistivity

Isotropic 2D joint inversion of CSEM and MT was performed to combine the benefits of high frequencies of CSEM and low frequencies of MT. The inversion image is shown in Figure 9, showing the structure of the basalt and resistive bodies, sediments underneath the basalt.

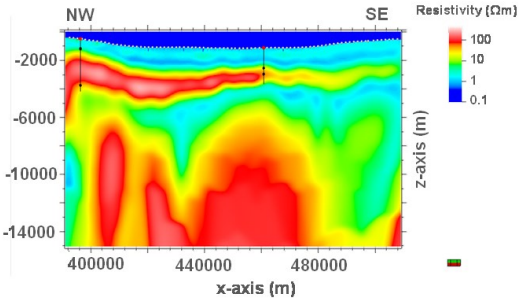

Figure 9: 2D CSEM+MT joint inversion from West of Shetland.

CSEM and joint inversion of CSEM+MT clearly image the base of basalt while not with MT as expected in this scenario. Finally we can say that all three inversions are consistent and reduce the uncertainty of basalt interpretations. The lateral variation and thickness of basalt is imaged properly. The well logs show that the EM results can resolve the complex geologic settings with confidence.

Conclusions

With anisotropic CSEM inversion, the properties of basalt can be found. MT is quite useful for thicker basalt and even the information about sediments below the basalt. The combination of the two methods utilizes the ability of the CSEM to image thin basalt while the imaging of the relative conductive sub-basalt sediments is improved by the MT data. This structural information can be helpful for seismic velocity model building and seismic imaging.

Seismic imaging is very challenging in sub-basalt regions. EM methods (CSEM + MT) can aid in imaging the base of basalt and the sediments underneath. Two scenarios were discussed; 1) synthetic data inversion for a realistic model, and, 2) a real field data example. Both cases provide convincing results for considering EM to improve sub-basalt exploration strategies.

Acknowledgements

The authors would like to thank EMGS and Statoil for permission to publish this work. We would also like to thank Friedrich Roth, Jason Tinder, Nikolay Golubev, Trude Støren and Volker Ullrich for helpful discussions.

References

Colombo, D., Keho, T. and McNeice, G., 2012, Integrated seismic-electromagnetic workflow for sub-basalt exploration in northwest Saudi-Arabia; The Leading Edge, 31, 42-52.

Constable, S.C., Parker, R.L., Constable, C.G., 1987, Occam's inversion- A practical approach for generating smooth models from electromagnetic sounding data; Geophysics, 52, 289-300.

Fliedner, M.M. and White, R.S., 2001, Seismic structure of basalt flows from surface seismic data, borehole measurements and synthetic seismogram modeling; Geophysics, 66, 1925-.

Hautot, S., Perrot, J., Jegen, M.D., Cairns, G., Tartis, P., 2002, Feasibility study of joint magnetotellurics/seismic interpretation for sub-basalt imaging; J. Conference Abstracts, 7, 150-151.

Herredsvela, J., Colpaert, A., Foss, S.-K., Nguyen, A.K., Hokstad, K., Morten, J.P., Twarz, C., Fanavoll, S. and Mrope, F., 2012, Feasibility of electromagnetic methods for sub-basalt exploration; SEG Las Vegas 2012 Annual Meeting.

Hoversten, G.M., Myer, D., Key, K., Hermann, O., Hobbet, R. and Alumbaugh, D., CSEM and MMT base basalt imaging; 75th EAGE Conference & Exhibition incorporating SPE EUROPEC 2013.

Jegen, M., Hautot, S., Cairns, G. and Tarits, P., 2002, Using electromagnetic to image sub-basalt sediments; J. Conference Abstracts, 7, 154-155.

Maaø, F., 2007, Fast Finite-difference time-domain modeling for marine-subsurface electromagnetic problems; Geophysics, 72, A19-A23.

MacGregor, L., 2003, Joint analysis of marine active and passive source EM data for sub-salt and sub-baslt imaging; 65th EAGE Conference & Exhibition, Expanded Abstracts, F18.

Morten, J.P., Fanavoll, S., Mrope, F.M. and Nguyen, A.K., 2011, Sub-basalt imaging using broadside CSEM; 73rd Conference & Exhibition, EAGE.

Thacher, C., Deeds, J., Stefani, J., Clark, D., Mitchell, P., Hermann, O., Hobbet, R., Alumbaugh, D. and Bevc, D., 2013, Sub-Volcanic 3D Modelling – North Atlantic Margin; 75th EAGE Conference & Exhibition incorporating SPE EUROPEC 2013.

Pandey, D.K., MacGregor, L.M., Sinha, M.C. and Singh, S.C., 2008, Feasibility of using magnetotellurics for sub-basalt imaging at kachchh, India; Applied Geophysics, 5, 74-82.